Simulating C_3-to-CAM transition under ancient atmospheric conditions

Devlina Sarkar and Sudip Kundu*

Department of Biophysics, Molecular Biology and Bioinformatics, University of Calcutta

92, APC Road, Kolkata 700009, India

*Corresponding author email: skbmbg@caluniv.ac.in

ORCID IDs- Devlina Sarkar: https://orcid.org/0009-0006-3979-4380

Sudip Kundu: https://orcid.org/0000-0003-1235-2540

No of figures in the main text- 2 (All the figures should be published in colour)

14 separate supporting information files (12 excel files, 1 sbml file and 1 text file) with the main SI pdf file

Abstract

Crassulacean Acid Metabolism (CAM) plants can survive in arid environment. CAM is hypothesized to evolve from C_3 metabolism about 20 to 30 million years ago (MYA) when the Earth faced declining atmospheric CO_2 concentration ($[CO_2]_a$), increasing aridity and decreasing temperature. Understanding whether and how these atmospheric changes favour C_3-to-CAM transition will help in engineering CAM into crop plants to tackle the threat of global climate change. Our simulations of plant cellular metabolism under the changing atmospheric conditions of ancient time observe C_3-to-CAM transition, capture possible temporal alterations of active metabolic pathways and further confirm that both the reduced $[CO_2]_a$ and increased water scarcity associated with higher aridity, can act as evolutionary agents, driving the C_3-to-CAM transition. Although the predicted elevated $[CO_2]_a$ of future reveals a reversion towards C_3-like behaviour, drought always favours CAM regardless of $[CO_2]_a$ and temperature levels. Moreover, a minimum oxygen concentration is needed to support higher nocturnal respiration, necessary for CAM.

Introduction

Crassulacean Acid Metabolism (CAM) plants can survive in arid environment. Time-calibrated phylogenies and large-scale carbon isotope ($\delta^{13}C$) studies suggest that CAM is evolved from C_3 about 20-30 million years ago (MYA) (Heyduk, 2022; Sage *et al.*, 2023). Evidences also suggest that during early-Eocene (56 MYA) to early-Miocene (20 MYA), atmospheric CO_2 concentration ($[CO_2]_a$) declined from 700-1000 ppm to about 200 ppm (Bellasio *et al.*, 2021; Sage *et al.*, 2023), Earth's surface temperature (T) decreased from ~35ºC to ~22ºC (Passchier *et al.*, 2013; Judd *et al.*, 2024); and aridification increased (Passchier *et al.*, 2013; Wang *et al.*, 2016) (i.e. relative humidity (RH) decreased from an initial value of ~67% in middle-Miocene (Jahren *et al.*, 2003)). Researchers hypothesized that the above-mentioned atmospheric changes during ancient times favour the evolution of CAM (Sage *et al.*, 2023).

Previous experimental efforts explored the physiological (Guan *et al.*, 2020) and molecular changes (Kong *et al.*, 2020), altered gene expressions (Heyduk *et al.*, 2019; Shen *et al.*, 2022), transcriptomic

(Cushman *et al.*, 2008; Brilhaus *et al.*, 2016) and proteomic (Guan *et al.*, 2021) changes, the roles of different phytohormones in controlling stomatal behaviour (Wakamatsu *et al.*, 2021) etc., during C_3-to-CAM transition in different facultative CAM species (Winter & Holtum, 2024) under different stress conditions (Tan & Chen, 2023). The different expression levels of carbonic anhydrase genes in *Arabidopsis thaliana* leaves were also reported under different atmospheric CO_2 concentrations (Rudenko *et al.*, 2022). On the other hand, several computational efforts simulated the C_3-to-CAM transition only in MC either by forcefully restricting the daytime CO_2 uptake (Tay *et al.*, 2021) or gradually reducing transpirational water loss accompanied by a trade-off in phloem sap production (Töpfer *et al.*, 2020). Recently, we developed a dual-cell (GC and MC) diel metabolic model, coupled with a gas diffusion model which links the CO_2 uptake to transpirational water loss, depending on the temporal fluctuations of T and RH (Sarkar & Kundu, 2025). Simulation showed gradual reduction of the transpirational water loss shifts the metabolism from C_3 to CAM and at the same time, captured the temporally differential activities of several enzymes involved in different pathways of central carbon metabolism, during this transition. However, none of these studies addressed whether and how atmospheric changes during early-Eocene to early-Miocene might have driven the shift from C_3 metabolism to CAM. Such insights will help in engineering CAM into crop plants to tackle the threat of global climate change and ensure food security (Lim *et al.*, 2025).

Here, we simulate our previously published six-phase GC-MC diel metabolic model (Sarkar & Kundu, 2025) of a plant leaf (**Supporting Information Fig. S1a**) using a constraint-based modelling approach (Flux Balance Analysis or FBA) (Orth *et al.*, 2010), under varying atmospheric conditions of that geological time period (**Supporting Information Fig. S1b-d**, for details, see **Materials and Methods**). Simulations observe C_3-to-CAM transition, capture possible temporal alterations of active metabolic pathways and further confirm that both the reduced $[CO_2]_a$ and increased water scarcity associated with higher aridity, can act as evolutionary agents, driving the C_3-to-CAM transition. While future's elevated $[CO_2]_a$ reveals a reversion towards C_3-like behaviour, drought always favours CAM regardless of $[CO_2]_a$ and temperature levels. Moreover, a minimum oxygen concentration is needed to support higher nocturnal respiration, necessary for CAM.

Materials and Methods

Model Description

Our previously constructed time-resolved atmospheric factors coupled metabolic model of a plant leaf is used here (Sarkar & Kundu, 2025). Briefly, this is a six-phase dual-cell (GC-MC) metabolic model coupled with transpirational water loss and CO_2 uptake [see **Supporting Information Fig. S1a**, equation (1) and equation (2)]. The transpirational water loss from the system in each phase depends on different environmental parameters such as temperature (T) and relative humidity (RH) of that particular phase. The six phases, denoted as p1 to p6, represent different time intervals of a diel cycle: dawn (0-1

h), mid-day (1-11 h), afternoon (11-12 h), evening (12-13 h), night (13-23 h) and pre-dawn (23-24 h) respectively. Thus, the 24-hour time span of a complete diel cycle is divided into these six phases in a ratio of 1:10:1:1:10:1. The equations of a gas diffusion model are given below.

$$J_{CO_2,available} = D_{CO_2} \frac{n\pi R^2}{l+R_{mean}} ([\mathrm{CO_2}]_i - [\mathrm{CO_2}]_a) \quad (1)$$

Equation 1 represents the flux of CO_2 ($J_{CO_2,available}$) that can enter the leaf's internal airspace through a stomatal pore of radius R at a specific concentration of atmospheric CO_2 ($[CO_2]_a$) and temperature (T). Moreover, $[CO_2]_i$ represents the concentration of CO_2 inside the leaf, D_{CO_2} is the diffusion coefficient of CO_2, n is the number of stomata per unit area of the leaf, πR^2 is the average area per stomatal pore, l is the depth of stomatal pore and R_{mean} is the mean radius which is added to the depth of the stomatal pore as a correction factor (Nobel, 2009). A plot of D_{CO_2} values at some particular temperatures, listed in Appendix I (Nobel, 2009), gives us a straight-line graph, showed in **Supporting Information Fig. S2**. We use linear regression method to get the c (intercept) and m (slope) of that straight line. Now, we can calculate D_{CO_2} values at specific temperatures of different phases of the diel cycle in different geological time periods. In a similar manner, we plot the internal CO_2 concentration of the leaf ($[CO_2]_i$) at different atmospheric CO_2 concentrations ($[CO_2]_a$) (>100 ppm) (Moss & Rawlins, 1963) and get the c (intercept) and m (slope) values using linear regression method. Using these values, we can calculate the $[CO_2]_i$ for any specific $[CO_2]_a$ value during early-Eocene to early-Miocene time period. The radius of the stomatal pore (R) at daytime is considered to be 7 µm with a basal value of 0.6 µm in the C_3 plant and the depth of the stomatal pore is considered to be twice the radius of the pore, assuming the pore to be circular, as used in our previously published work (Sarkar & Kundu, 2025). The number of stomata per mm^2 is considered to be 250, which is within the reported values, ranging from 45 to 720 (Hetherington & Woodward, 2003).

$$J_{H_2o} = k\left(c(T)^*_{i,H_2o} - c(T)^*_{a,H_2o}.RH\right).J_{CO_2,demand} \quad (2)$$

$$\text{where, } k = \frac{D^0_{H_2O}}{D^0_{CO_2}} . \frac{1}{[\mathrm{CO_2}]_i - [\mathrm{CO_2}]_a}$$

Equation 2 gives us the relationship between the water loss through transpiration and the CO_2 demand of the system depending on the T and RH in each phase throughout the diel cycle. The values of T and RH for different phases of a diel cycle are estimated using a skewed sinus generator[7]. $c(T)^*_{H_2o}$ is the saturation concentration of water vapour, $D^0_{H_2o}$ and $D^0_{CO_2}$ are the standard diffusion coefficients of H_2O and CO_2, and ($[CO_2]_i$ - $[CO_2]_a$) is the concentration difference of CO_2 inside and outside the leaf. We convert the values of concentration of CO_2 ($[CO_2]$) from ppm to $\mu mol.m^{-3}$ to use in our simulation.

The metabolisms of GC and MC are interlinked in this model in a very simple way. The accumulation of osmolytes in GC opens stomata. Equation 1 gives us the maximum flux of CO_2 that can enter the system depending on the size of stomatal pore, diffusion coefficients at different temperatures in different phases of the diel cycle and the concentration difference of CO_2 inside and outside the leaf. The amount of CO_2 entering each phase is further scaled by multiplying it with the duration of that

phase. The entered CO_2 is available to 300 MCs and 1 GC in the internal space of the leaf as the ratio of MC to GC is considered to be 300, as used in our previous study (Sarkar & Kundu, 2025). On the other hand, MC supplies sucrose to GC, which ultimately helps in stomatal opening. Sucrose is allowed to transfer from MC to GC in phase 2 at daytime and in phase 5 at nighttime. The rate of solute accumulation (i.e, osmotic pressure or OP) is 1.928 $\mu osmol.m^{-2}.s^{-1}$ for 7 μm aperture size (Sarkar & Kundu, 2025). Assuming the photosynthetic capacity of GC to be 20%, the amount of sucrose transferred to GC is 80% of the OP, as previously used (Sarkar & Kundu, 2025). In the model, ions (K^+, Cl^-, H^+) can move in and out of GC during any phase of the day or night. However, experimental studies have shown that K^+ accumulates in GC primarily during early morning, while sucrose accumulation takes place later during the day (Lawson, 2009). Based on this, the transfer of K^+ from phase 2 to phase 3 is blocked in the model. The schematic representation of the model is shown in **Supporting Information Fig. S1a,** the model files are provided in the **Supporting Information Datasets S1** and **S2**; and all the other constraints are listed in the **Supporting Information Table S1.** The constraints, which we have taken from our previously published paper (Sarkar & Kundu, 2025), are based on various experimental observations (see references therein).

Simulating the model with the changing atmospheric conditions during early-Eocene to early-Miocene period

It is reported that $[CO_2]_a$ declined from 700-1000 to 200 ppm (Bellasio *et al.*, 2021; Sage *et al.*, 2023), T decreased from 35-22ºC (Passchier *et al.*, 2013; Judd *et al.*, 2024) and RH decreased (Passchier *et al.*, 2013; Wang *et al.*, 2016) during the early-Eocene to early-Miocene time period. There is no report about the values of RH in early-Eocene and early-Miocene, whereas it is reported to be 67% in the middle Eocene (Jahren *et al.*, 2003). However, several studies reported the reduction of RH during this time interval (Passchier *et al.*, 2013; Wang *et al.*, 2016). Therefore, we consider the value of RH in early-Eocene and early-Miocene to be 70% and 30%, higher and lower than that in middle-Eocene respectively. We use some known physiological parameters for C_3 and CAM, already used in our previous work (Sarkar & Kundu, 2025) and here, those are listed in **Supporting Information Table S1**. Some constraints like ratio of photon values in different phases of day, percentage of sucrose transferred from MC to GC in phase 2 and phase 5 etc., remain unchanged throughout the simulation from early-Eocene to early-Miocene time period. However, to implement the higher CO_2 concentration around RuBisCO in CAM, the ratio of carboxylase and oxygenase activities of RuBisCO is assumed to gradually increase from 3 to 5.15 (Tay *et al.*, 2021; Sarkar & Kundu, 2025) during this geological time period. There is no data available about the temporal variation of T and RH in ancient times and therefore, we assume the difference of max and min T and RH to be 10ºC and 10% respectively. Experimental evidences showed that the maximum stomatal apertures for basil and broad bean are 7 μm and 7.4 ± 2.3 μm respectively (Outlaw & De Vlieghere-He, 1992; Kang *et al.*, 2007). In our previously published model (Sarkar & Kundu, 2025), the starting aperture size of the simulation during

all three daytime phases was set to 7 µm. A basal value of 0.6 µm during all the six phases was considered. But we did not impose any upper limit on stomatal opening. In the present study, however, we allow the aperture size to increase up-to 7µm, above the basal stomatal opening of 0.6 µm, resulting in a maximum aperture size of 7.6 µm at any phase, which lies within the reported experimental range. As there was a majority of C_3 plants on the Earth before Oligocene or Miocene period (Sage *et al.*, 2023), we start the simulation using the constraints of C_3 metabolism under the atmospheric condition of early-Eocene period with the average T of 35°C, RH of 70% and $[CO_2]_a$ of 800 ppm (**Supporting Information Fig. S1b-d**). Next, we gradually decrease the $[CO_2]_a$, T and RH until the values reach to 250 ppm, 22°C and 30% respectively, representing the atmospheric condition of the early-Miocene period and simulate the model at each step (**Supporting Information Fig. S1b-d**). Here, a 2-step iteration method is used for simulating the model at a single geological time point. Steps for simulating the model under the changing atmospheric conditions between early-Eocene to early-Miocene time period are shown in **Supporting Information Fig. S1d**.

Simulating the model with gradual reduction in transpirational water loss at each step of atmospheric changes between early-Eocene to early-Miocene period

To check the effect of water scarcity at different geological time points, we simulate the model by gradually reducing transpirational water loss at every point of the atmospheric changes between early-Eocene to early-Miocene time period. Steps of this simulation are given in **Supporting Information Fig. S1e.**

Calculating the correlation of the flux values through the metabolic reactions with changing atmospheric conditions and reduced transpirational water loss

The rank correlation between the flux values of each reaction of the model- i) with the change in atmospheric conditions during early-Eocene to early-Miocene time period (gradual reduction in $[CO_2]_a$, T and RH) and ii) with the reduction in transpirational water loss at each point between that geological time period are calculated using in-house python scripts (**Supporting Information Dataset S3**).

Simulating the model at different combinations of $[CO_2]_a$, T and RH

To check the response of plant metabolism in changing atmospheric conditions of future, we simulate the model by reducing the RH from 80% to 40% (with a decrement of 10%) at different combinations of $[CO_2]_a$ (800, 419 and 250 ppm) and T (26-35ºC with an increment of 1ºC). These simulations are performed- i) with unconstrained transpirational water loss and ii) with the transpirational water loss fixed at a value obtained by simulating the model with 80% RH for specific T and $[CO_2]_a$ combination. For example, at a given $[CO_2]_a$ of x ppm and T of y ºC, the first simulation involves reducing RH from 80% to 40% with unconstrained transpirational water loss. Whereas, in the second simulation, RH is similarly reduced from 80% to 40% at the same $[CO_2]_a$ and T; but in each step, transpirational water loss is fixed at the value obtained from simulating the model under $[CO_2]_a$ = x ppm, T = y ºC and RH =

80%. Here, we have started the simulation with full opening of stomata in all the six phases of diel cycle. Depending on the specific atmospheric condition, i.e., specific combination of $[CO_2]_a$, T and RH values, the phase-specific CO_2 import is predicted and the aperture size and OP are readjusted.

Simulating the model at $[CO_2]_a$ of 250 ppm with reduced phloem sap production

At $[CO_2]_a$ of 250 ppm, we start with the rate of phloem sap production to be 0.259 $\mu mol.m^{-2}.^{-1}$. Then for each T and RH combination, we gradually decrease the production rate by 20%, keeping all the other constraints unchanged and simulate the model at each step using the 2-step iteration method (described earlier).

Flux Balance Analysis (FBA)

We have used Flux Balance Analysis (FBA) (Orth *et al.*, 2010), a constraint-based modelling approach for simulating our model. In this approach, the reactions of the metabolic model are represented in the form of a stoichiometry matrix, **S** of size m x n, where m represents the number of metabolites and n represents the number of reactions present in the model. At steady state, the rate of production and the rate of consumption are equal for each internal metabolite in the model. This can be mathematically represented as,

$$\mathbf{Sv} = 0.$$

where, the vector **v** represents the flux through all the n number of reactions and **S** is the stoichiometry matrix.

The optimization problem can be defined as,

$$\text{maximize or minimize } \mathbf{z} = \mathbf{c}^T\mathbf{v}$$

where, **z** is the objective function, $\mathbf{c}^T$ is the transpose of a vector (**c**) of weights that indicate how much a reaction contributes to the objective, **v** is the vector of all fluxes.

The constraints on the flux values are given as,

$$\mathbf{c}_l \leq \mathbf{v} \leq \mathbf{c}_u$$

where, **v** is the vector of all fluxes, and $\mathbf{c}_u$ and $\mathbf{c}_l$ are the upper and lower bounds of fluxes, respectively. The objective used in this study is minimization of the total absolute sum of fluxes (proxy of minimization of cellular economy). The scobra package (Shaw & Cheung, 2018) is used for simulations of FBA. The codes for all the simulations are given in **Supporting Information Dataset S3.**

Results and Discussion

Atmospheric changes during early-Eocene to early-Miocene favour the C_3-to-CAM transition

Simulating the model under the atmospheric condition of early-Eocene period confirms the important characteristics of C_3 metabolism- such as CO_2 uptake only at daytime (Winter & Smith, 2022), malate storage at daytime in MC (Winter & Smith, 2022), early morning K^+ storage in GC (Daloso *et al.*, 2017) and sucrose storage in the later phases of the day in GC (Daloso *et al.*, 2017) etc. Then, as we move towards early-Miocene by gradually reducing $[CO_2]_a$, T and RH, the metabolism begins to exhibit key

features of CAM (Winter & Smith, 2022) (**Supporting Information Dataset S4**)- i) CO_2 uptake at night (**Fig. 1a**) through nighttime GC-mediated stomatal opening (**Fig. 2e, Supporting Information Fig. S3**), ii) the increased activities of some C_4-like enzymes such as PEPC (phosphoenolpyruvate carboxylase) and MDH (malate dehydrogenase) at nighttime, whereas PEPCK (phosphoenolpyruvate carboxykinase) and NADP-ME (NADP-dependent malic enzyme) at daytime in MC (**Fig. 1b**); and iii) the increased daytime starch and nighttime malate storages in MC (**Fig. 1c**). Although nocturnal CO_2 uptake begins around 419 ppm (**Fig. 1a**), nighttime malate accumulation starts earlier (**Fig. 1c**). In response to decline in $[CO_2]_a$, plant initially adjusts its metabolism by limiting daytime CO_2 uptake and refixing respiratory CO_2 into malate at night. As $[CO_2]_a$ drops further, it starts taking atmospheric CO_2 at night to meet the total carbon requirement, in addition to respiratory CO_2 fixation (Griffiths *et al.*, 1989). CAM-like features gradually emerge as we move towards the Miocene, but the typical stomatal pattern with complete midday closure (Heyduk, 2022; Sarkar & Kundu, 2025) is not observed here. With CAM emergence, nocturnal respiration increases through elevated O_2 uptake, enhanced TCA fluxes (**Fig. 1d**, **Supporting Information Dataset S4, Supporting Information Note S1**), and increased mitochondrial ATP production, supplying essential energy for CAM. Additionally, simulation with restricted nighttime O_2 uptake reveals that increased nocturnal O_2 uptake is mandatory for CAM functioning, supporting the experimental observation that CAM requires elevated nocturnal respiratory rate and nocturnal O_2 consumption (Leverett & Borland, 2023). Interestingly, atmospheric O_2 concentration increased during that geological time period (Berner *et al.*, 2007), which probably supports the higher O_2 consumption and facilitated the emergence of CAM. Furthermore, as we move towards Miocene, there is an overall decrease in water-use efficiency (WUE) (**Fig. 1d**) due to increase in transpirational water loss. This result is consistent with earlier experimental reports suggesting that plants cope with the lower $[CO_2]_a$ by opening stomata and therefore stomatal conductance increases (Sage *et al.*, 2023). This consequently increases the transpiration rate and hence WUE decreases (Sage *et al.*, 2023).

Both $[CO_2]_a$ and aridity can act as evolutionary agents for the C_3-to-CAM transition

Now, to identify the major atmospheric changes that favour C_3-to-CAM transition, we study the response of plant C_3 metabolism at higher $[CO_2]_a$ (800 ppm), but at different T (35ºC to 22 ºC) and RH (70% to 30%) (**Supporting Information Dataset S5**). Interestingly, we observe variations of T and RH, alone or in combination, are not sufficient to drive the C_3-to-CAM transition. We already show that the transition is favoured when changes in T and RH are coupled with lower $[CO_2]_a$ (**Fig. 1a**). Moreover, when we simulate the C_3 metabolism at reducing $[CO_2]_a$ only, keeping the T and RH fixed at 35ºC and 70% respectively, we observe the C_3-to-CAM transition (**Supporting Information Dataset S6**). These support the hypothesis that lower $[CO_2]_a$ during ancient times drives the C_3-to-CAM transition (Sage *et al.*, 2023).

We should note that we have not restricted the transpirational water loss in our earlier simulations to nullify the effect of reduced water loss during C_3-to-CAM transition established by previous studies (Töpfer *et al.*, 2020; Sarkar & Kundu, 2025). However, the increased aridity of early-Miocene is expected to be associated with reduced water availability and this water scarcity is also supported by the disappearance of lakes caused by aridity (Wang *et al.*, 2023) during various geological periods. As reduction in transpirational water loss is one of the ways to adapt and survive at water-stressed conditions, we gradually reduce the transpirational water loss at different points between early-Eocene to early-Miocene (**Supporting Information Fig. S1e**) and observe a metabolic shift to CAM regardless of whether $[CO_2]_a$ is high or low (**Supporting Information Dataset S4**). We also observe the shift in stomatal opening from day to night (**Fig. 2e, Supporting Information Fig. S3**), maximum CO_2 uptake at night (**Fig. 2a,b, Supporting Information Fig. S4**), higher activities of PEPC, PEPCK, MDH and NADP-ME (**Fig. 2c,d, Supporting Information Fig. S5**), and increased storages of starch and malate at day and night respectively (**Supporting Information Fig. S6**). These findings support the fact that water stress causes C_3-to-CAM transition even at higher CO_2 (Sage *et al.*, 2023). Various studies have suggested that both factors could drive the C_3-to-CAM transition (Silvera *et al.*, 2010; Sage *et al.*, 2023) and metabolic modelling also support the fact. However, the transition also demands substantial cellular and genetic modifications, which would further influence its evolutionary pathway.

Interestingly, WUE increases when associated with the limitation in transpirational water loss at any point between early-Eocene and early-Miocene (**Supporting Information Fig. S7**). Moreover, as reduction in transpirational water loss (or water saving) diminishes with decline in $[CO_2]_a$, the extent of WUE improvement due to reduced water loss, is also reduced. It is also important to note that at higher $[CO_2]_a$, where higher water saving is possible, midday stomatal closure is observed (**Fig. 2e, Supporting Information Fig. S3**). The rank correlation values between reaction's flux and atmospheric changes from the early-Eocene to early-Miocene, or with reduced transpiration water loss at each point within this interval, indicate that MC metabolism shifts similarly during the C_3-to-CAM transition in both cases, whereas GC displays different patterns (**Supporting Information Dataset S7, Supporting Information Note S2**).

Impact of future atmospheric changes on metabolism

One of the major reasons of CAM emergence is reduced $[CO_2]_a$. However, after the industrial revolution, $[CO_2]_a$ increased roughly by 40%, from a value of 278 ppm (Asadi Zarch *et al.*, 2017). It continues to increase day by day and is predicted to increase further in near future (Asadi Zarch *et al.*, 2017). Model simulations under elevated $[CO_2]_a$ show enhanced daytime CO_2 uptake and reduced nocturnal fixation (**Supporting Information Table S2**), aligning with experimental findings (Sage *et al.*, 2023). Simulations under varying $[CO_2]_a$, T, and RH reveal that water loss rises with higher T, lower $[CO_2]_a$, and reduced RH (**Fig. 2f**). Moreover, for a fixed T and $[CO_2]_a$, imposing water-saving

constraints along with reduced RH induces CAM, with greater nocturnal CO_2 uptake (**Fig. 2g, Supporting Information Dataset S8**). At high $[CO_2]_a$, plants shift CO_2 uptake to cooler nights due to reduced transpirational water loss without reducing phloem sap. Whereas at low $[CO_2]_a$, limited CO_2 forces nocturnal uptake and further reduction in transpirational water loss compromises phloem sap production, reflecting a trade-off between water saving and phloem sap production (**Fig. 2g, Supporting Information Dataset S9**). For details, see **Supporting Information Note S3**.

Extended model also confirms the C_3-to-CAM transition

In our model, K_2malate, KCl and sucrose are initially considered as osmolytes (Talbott & Zeiger, 1996; Lawson, 2009; Daloso *et al.*, 2016, 2017; Santelia & Lawson, 2016; Robaina-Estévez *et al.*, 2017), with only sucrose permitted to transfer from MC to GC (Lawson *et al.*, 2014; Daloso *et al.*, 2016). We now extend the model to include additional osmolytes (nitrate, glucose, fructose and maltose) in GC and transfer metabolites (glucose and malate) from MC to GC (Talbott & Zeiger, 1993; Lawson *et al.*, 2014; Daloso *et al.*, 2017; Flütsch *et al.*, 2020b,a; Dang *et al.*, 2024) (**Supporting Information Dataset S10**). Simulations of this extended model also indicate that, even with these inclusions, declining $[CO_2]_a$ and rising aridity consistently drive a metabolic shift toward CAM. While, MC shows similar metabolic patterns, GC shows variation in the storage patterns of these osmolytes for generating turgor pressure (**Supporting Information Note S4, Supporting Information Dataset S11**).

Simulating with other biological goal

Moreover, we have simulated our model using a dual objective function- maximization of phloem sap production followed by minimization of total absolute sum of the flux values (proxy of the cellular economy). Initially, we fix the RuBisCO's carboxylase-to-oxygenase activity ratio at 3 and simulate the model under the changing atmospheric conditions during early-Eocene to early-Miocene (**Supporting Information Dataset S12**). These simulations observe the metabolic shift from C_3 to CAM. We also simulate the model with the RuBisCO's carboxylase-to-oxygenase activity ratio fixed at 5.15:1 (Luttge, 2010, Shameer *et al.*, 2018) under the ancient atmospheric condition of early-Eocene and the results show that the ratio of 5.15:1 alone does not induce the CAM pathway (**Supporting Information Dataset S13**). It indicates that the different RuBisCO's carboxylase-to-oxygenase activity ratios alone do not drive the metabolic shift to CAM. Instead, the transition is primarily induced by changes in the ancient atmospheric conditions. Further, for incorporating the known physiological conditions of C_3 and CAM in our constraint-based simulation, we gradually increased the ratio from 3:1 to 5.15:1 (**Supporting Information Dataset S14**). We should note that the ratio of RuBisCO's carboxylase-to-oxygenase activity, 3:1 (Gutteridge and Pierce, 2006) and 5.15:1 (Luttge, 2010) are experimentally observed values for C_3 and CAM respectively. Moreover, a previous computational study of C_3 to CAM transition of mesophyll cell (Tay *et al.,* 2021) also used a changing ratio of RuBisCO's carboxylase-to-

oxygenase activity. The simulation of the model with changing ratio of RuBisCO's carboxylase-to-oxygenase activity also predicts a shift from C_3 metabolism to CAM. The results show patterns similar to those in **Figs 1** and **2** and the **Supporting Information Figs S1-7**. Hönisch *et al*., 2023 says- "All major Cenozoic CAM diversification events coincided with intervals when CO_2 was lower than ~430 ppm". Consistent with this, our simulation indicates that the model begins to take up CO_2 at night at around 462 ppm. Additionally, at any specific point in the ancient timeline, restricting transpirational water loss also induces the transition from C_3 to CAM metabolism.

Simulating the model with varying stomatal density and varying RH values during that geological time period

Research suggests that species differ in how stomatal density responds to elevated atmospheric CO_2 concentration ($[CO_2]_a$)- some increasing, some decreasing, and others showing none or only minor changes (Serna, 2008). We now aim to examine how the outcomes of our simulations depend on these different stomatal density responses under varying $[CO_2]_a$. Several species exhibit no change in stomatal density in response to elevated $[CO_2]_a$ (Woodward, 1995, Oberbauer et al., 1985, Radoglou *et al.,* 1990, Radoglou *et al.,* 1992, Ferris *et al.,* 1994, Apple *et al.,* 2000, Serna *et al.,* 2000). All the previous results presented in this study are based on simulations assuming constant stomatal density across changing $[CO_2]_a$. In some other plants, stomatal density increases with declining $[CO_2]_a$ (Woodward, 1987; Woodward & Bazzaz, 1988; Woodward & Kelly**,** 1995). To incorporate this into our analysis, we simulate the model by gradually increasing stomatal density from 250 mm^{-2} as $[CO_2]_a$ declined. Results show that higher stomatal density allows greater daytime CO_2 uptake at each $[CO_2]_a$ level compared with our previous results, leading to a delayed transition from C_3 to CAM metabolism in the ancient time scale. In some other species, stomatal density decreases with the decrease in $[CO_2]_a$ (Woodward & Kelly**,** 1995, Ferris *et al.,* 1994, Driscoll *et al.,* 2005). To evaluate this scenario, we simulated our model by gradually decreasing stomatal density from 250 mm^{-2} as $[CO_2]_a$ declined. The results show that lower stomatal density reduces daytime CO_2 availability compared with our previous simulations, causing the shift from C_3 to CAM metabolism to occur earlier in the geological time scale.

It should be noted that RH values for the early-Eocene and early-Miocene are not available, whereas the middle Eocene RH has been estimated to be 67% (Jahren *et al.*, 2003). Several studies indicate that RH declined over this time interval (Passchier *et al.*, 2013; Wang *et al.*, 2016). Therefore, initially we have used RH values of 70% for the early-Eocene and 30% for the early-Miocene, representing conditions slightly higher and lower than those of the middle Eocene, respectively. However, due to the lack of precise RH estimates for these ancient periods, we have also conducted simulations using different RH values of early-Eocene and early-Miocene to test how changes in RH influence the model outcomes. The results indicate that even with a variation in the upper (RH during early-Eocene) and lower (RH during early-Miocene) bounds of relative humidity (RH), the model consistently predicts a

transition from C_3 to CAM metabolism. Although transpirational water loss changes in response to RH fluctuations, the overall conclusions of the study remain unchanged.

To summarize, although anatomical and physiological traits such as increased succulence in CAM plants (Lüttge, 2004), stomatal regulation by differential activities of signalling pathways (Blatt, 2000), mechanistic regulation of stomata (Blatt *et al.*, 2022), change in assimilation rate with atmospheric conditions (Rudenko *et al.*, 2022) etc., are not included in our model; this environment-coupled simple cellular metabolic model successfully reconstructs ancient conditions, captures the C_3-to-CAM transition driven by environmental changes during that geological time period and provide an initial useful framework to predict the possible differentially active metabolic pathways and quantitative estimations of relative flux values through those in the changing environment, a requisite for proper designing of abiotic stress tolerant cultivar.

References

Apple ME, Olszyk DM, Ormrod DP, Lewis J, Southworth D, Tingey DT. 2000. Morphology and stomatal function of Douglas fir needles exposed to climate change: Elevated CO2 and temperature. *International Journal of Plant Sciences* **161**: 127-132.

Asadi Zarch MA, Sivakumar B, Malekinezhad H, Sharma A. **2017**. Future aridity under conditions of global climate change. *Journal of Hydrology* **554**: 451–469.

Bellasio C, Quirk J, Ubierna N, Beerling DJ. **2021**. Physiological responses to low CO2 over prolonged drought as primers for forest–grassland transitions. *Nature Plants* **8**: 1014–1023.

Berner RA, VandenBrooks JM, Ward PD. **2007**. Oxygen and evolution. *Science* **316**: 557–558.

Blatt MR. **2000**. Cellular signaling and volume control in stomatal movements in plants. *Annual review of cell and developmental biology* **16**: 221-241.

Blatt MR, Jezek M, Lew VL, Hills A. **2022**. What can mechanistic models tell us about guard cells, photosynthesis, and water use efficiency? *Trends in Plant Science* **27**: 166–179.

Brilhaus D, Bräutigam A, Mettler-Altmann T, Winter K, Weber APM. **2016**. Reversible burst of transcriptional changes during induction of crassulacean acid metabolism in Talinum triangulare. *Plant Physiology* **170**: 102–122.

Cenozoic CO2 Proxy Integration Project (CenCO2PIP) Consortium*†, Hönisch B, Royer DL, Breecker DO, Polissar PJ, Bowen GJ, Henehan MJ, Cui Y, Steinthorsdottir M, McElwain JC and Kohn MJ, 2023. Toward a Cenozoic history of atmospheric CO2. *Science*, ***382***(6675): eadi5177.

Cushman JC, Tillett RL, Wood JA, Branco JM, Schlauch KA. **2008**. Large-scale mRNA expression profiling in the common ice plant, Mesembryanthemum crystallinum, performing C3 photosynthesis and Crassulacean acid metabolism (CAM). *Journal of Experimental Botany* **59**: 1875–1894.

Daloso DM, dos Anjos L, Fernie AR. **2016**. Roles of sucrose in guard cell regulation. *New Phytologist* **211**: 809–818.

Daloso DM, Medeiros DB, dos Anjos L, Yoshida T, Araújo WL, Fernie AR. **2017**. Metabolism within the specialized guard cells of plants. *New Phytologist* **216**: 1018–1033.

Dang T, Piro L, Pasini C, Santelia D. **2024**. Starch metabolism in guard cells: At the intersection of environmental stimuli and stomatal movement. *Plant Physiology*, **196**: 1758-1777.

Driscoll SP, Prins A, Olmos E, Kunert KJ, Foyer CH. 2005. Specification and adaxial and abaxial stomata, epidermal structure and photosynthesis to CO2 enrichment in maize leaves. *Journal of Experimental Botany* **572**: 381-390.

Ferris R, Taylor G. 1994. Stomatal characteristics of four native herbs following exposure to elevated CO2. *Annals of Botany* **73**: 447-453.

Flütsch S, Nigro A, Conci F, Fajkus J, Thalmann M, Trtílek M, Panzarová K, Santelia D. **2020a**. Glucose uptake to guard cells via STP transporters provides carbon sources for stomatal opening and plant growth. *EMBO reports* **21**: e49719.

Flütsch S, Wang Y, Takemiya A, Vialet-Chabrand SRM, Klejchová M, Nigro A, Hills A, Lawson T, Blatt MR, Santelia D. **2020b**. Guard cell starch degradation yields glucose for rapid stomatal opening in Arabidopsis. *Plant Cell* **32**: 2325–2344.

Griffiths H, Ong BL, Avadhani PN, Goh CJ. **1989**. Recycling of respiratory C02 during Crassulacean acid metabolism: alleviation of photoinhibition in *Pyrrosia piloselloides*. *Planta* **179**: 115-122.

Guan Q, Kong W, Zhu D, Zhu W, Dufresne C, Tian J, Chen S. **2021**. Comparative proteomics of Mesembryanthemum crystallinum guard cells and mesophyll cells in transition from C3 to CAM. *Journal of Proteomics* **231**: 104019.

Guan Q, Tan B, Kelley TM, Tian J, Chen S. **2020**. Physiological Changes in Mesembryanthemum crystallinum During the C3 to CAM Transition Induced by Salt Stress. *Frontiers in Plant Science* **11**: 283.

Gutteridge S, and Pierce J. 2006. A unified theory for the basis of the limitations of the primary reaction of photosynthetic CO2 fixation: was Dr. Pangloss right? *Proceedings of the National Academy of Sciences of the United States of America*. **103**: 7203–7204.

Hetherington AM, Woodward & FI. **2003**. The role of stomata in sensing and driving environmental change. *Nature* **424**: 901-908.

Heyduk K. **2022**. Evolution of Crassulacean acid metabolism in response to the environment: past, present, and future. *Plant Physiology* **190**: 19–30.

Heyduk K, Hwang M, Albert V, Silvera K, Lan T, Farr K, Chang TH, Chan MT, Winter K, Leebens-Mack J. **2019**. Altered gene regulatory networks are associated with the transition from C 3 to crassulacean acid metabolism in erycina (Oncidiinae: Orchidaceae). *Frontiers in Plant Science* **9**: 2000.

Jahren AH, Silveira L, Sternberg L. **2003**. Humidity estimate for the middle Eocene Arctic rain forest. *Geology*, **31**: 463-466.

Judd EJ, Tierney JE, Lunt DJ, Montañez IP, Huber BT, Wing SL, Valdes PJ. **2024**. A 485-million-year history of Earth's surface temperature. *Science (New York, N.Y.)* **385**: eadk3705.

Kang Y, Outlaw WH, Fiore GB, Riddle KA. **2007**. Guard cell apoplastic photosynthate accumulation corresponds to a phloem-loading mechanism. *Journal of Experimental Botany* **58**: 4061–4070.

Kong W, Yoo MJ, Zhu D, Noble JD, Kelley TM, Li J, Kirst M, Assmann SM, Chen S. **2020**. Molecular changes in Mesembryanthemum crystallinum guard cells underlying the C3 to CAM transition. *Plant Molecular Biology* **103**: 653–667.

Lawson T. **2009**. Guard cell photosynthesis and stomatal function. *New Phytologist* **181**: 13–34.

Lawson T, Simkin AJ, Kelly G, Granot D. **2014**. Mesophyll photosynthesis and guard cell metabolism impacts on stomatal behaviour. *New Phytologist* **203**: 1064–1081.

Leverett A, Borland AM. **2023**. Elevated nocturnal respiratory rates in the mitochondria of CAM plants: current knowledge and unanswered questions. *Annals of Botany* **132**: 855–867.

Lim SD, Lomas JS, Islam M, Pérez-López A V., Kim SH, Petrusa LM, Yim WC, Cushman JC. **2025**. Synthetic crassulacean acid metabolism (SynCAM) for improving water-use efficiency in plants. *Philosophical Transactions of the Royal Society B: Biological Sciences* **380**: 20240249.

Lüttge U. **2004**. Ecophysiology of Crassulacean Acid Metabolism (CAM). *Annals of Botany* **93**: 629–652.

Lüttge, U. 2010. Photorespiration in phase III of crassulacean acid metabolism: evolutionary and ecophysiological implications. *Progress in Botany*. **72**: 371–384.

Moss DN, Rawlins SL. **1963**. Concentration of Carbon Dioxide inside Leaves. *Nature*. **197**: 1320-1321.

Nobel PS. **2009**. Physicochemical and Environmental Plant Physiology. In: Physicochemical and Environmental Plant Physiology. Elsevier, 364–437.

Oberbauer SF, Strain BR, Fetcher N. 1985. Effect of CO2-enrichment on seedling physiology and growth of two tropical tree species. *Physiologia Plantarum* **65**: 352-356.

Orth JD, Thiele I, Palsson BO. **2010**. What is flux balance analysis? *Nature Biotechnology* **28**: 245–248.

Outlaw WH, De Vlieghere-He X. **1992**. Transpiration Rate. An Important Factor Controlling the Sucrose Content of the Guard Cell Apoplast of Broad Bean. *Plant Physiology* **126**: 1716-1724

Passchier S, Bohaty SM, Jiménez-Espejo F, Pross J, Röhl U, Van De Flierdt T, Escutia C, Brinkhuis H. **2013**. Early eocene to middle miocene cooling and aridification of east antarctica. *Geochemistry, Geophysics, Geosystems* **14**: 1399–1410.

Radoglou KM, Jarvis PG. 1990. Effects of CO2 enrichment on four poplar clones. II. Leaf surface properties. *Annals of Botany* **65**:627-32.

Radoglou KM, Jarvis PG. 1992. The effects of CO2 enrichment and nutrient supply on growth morphology and anatomy of Phaseolus vulgaris L. seedlings. *Annals of Botany* **70**: 245-256.

Robaina-Estévez S, Daloso DM, Zhang Y, Fernie AR, Nikoloski Z. **2017**. Resolving the central metabolism of Arabidopsis guard cells. *Scientific Reports* **7**: 8307.

Rudenko NN, Ignatova LK, Naydov IA, Novichkova NS, Ivanov BN. **2022**. Effect of CO2 Content in Air on the Activity of Carbonic Anhydrases in Cytoplasm, Chloroplasts, and Mitochondria and the Expression Level of Carbonic Anhydrase Genes of the α- and β-Families in Arabidopsis thaliana Leaves. *Plants* **11**: 2113.

Sage RF, Gilman IS, Smith JCA, Silvera K, Edwards EJ. **2023**. Atmospheric CO2 decline and the timing of CAM plant evolution. *Annals of Botany* **132**: 753–770.

Santelia D, Lawson T. **2016**. Rethinking guard cell metabolism. *Plant Physiology* **172**: 1371–1392.

Sarkar D, Kundu S. **2025**. Water-saving guard cell-mesophyll cell model captures temporally differential enzymatic and transporter activities during C3-crassulacean acid metabolism transition. *Plant physiology* **197**: kiaf048.

Serna L, Fenoll C. 2000. Plant Biology: Coping with human CO2 emissions. *Nature* **408**: 656-657.

Serna L, 2008. Drawing the future: Stomatal response to CO2 levels. *Plant Signaling & Behavior*, *3*(4), 214-217.

Shameer S, Baghalian K, Cheung CM, Ratcliffe RG and Sweetlove LJ. 2018. Computational analysis of the productivity potential of CAM. *Nature Plants*, ***4***(3), 165-171.

Shaw R, Cheung CYM. **2018**. A dynamic multi-tissue flux balance model captures carbon and nitrogen metabolism and optimal resource partitioning during arabidopsis growth. *Frontiers in Plant Science* **9**: 884.

Shen S, Li N, Wang Y, Zhou R, Sun P, Lin H, Chen W, Yu T, Liu Z, Wang Z, *et al.* 2022. High-quality ice plant reference genome analysis provides insights into genome evolution and allows exploration of genes involved in the transition from C3 to CAM pathways. *Plant Biotechnology Journal* **20**: 2107–2122.

Silvera K, Neubig KM, Whitten WM, Williams NH, Winter K, Cushman JC. **2010**. Evolution along the crassulacean acid metabolism continuum. *Functional Plant Biology* **37**: 995–1010.

Talbott LD, Zeiger E. **1993**. Sugar and Organic Acid Accumulation in Guard Cells of Vicia faba in Response to Red and Blue Light. *Plant Physiology*, **102**: 1163-1169.

Talbott LD, Zeiger E. **1996**. Central Roles for Potassium and Sucrose in Guard-Cell Osmoregulation. *Plant physiology*, **111**: 1051-1057.

Tan B, Chen S. **2023**. Defining Mechanisms of C3 to CAM Photosynthesis Transition toward Enhancing Crop Stress Resilience. *International Journal of Molecular Sciences* **24**: 13072.

Tay IYY, Odang KB, Cheung CYM. **2021**. Metabolic Modeling of the C3-CAM Continuum Revealed the Establishment of a Starch/Sugar-Malate Cycle in CAM Evolution. *Frontiers in Plant Science* **11**: 573197.

Töpfer N, Braam T, Shameer S, Ratcliffe RG, Sweetlove LJ. **2020**. Alternative crassulacean acid metabolism modes provide environment-specific water-saving benefits in a leaf metabolic model. *Plant Cell* **32**: 3689–3705.

Wakamatsu A, Mori IC, Matsuura T, Taniwaki Y, Ishii R, Yoshida R. **2021**. Possible roles for phytohormones in controlling the stomatal behavior of Mesembryanthemum crystallinum during the salt-induced transition from C3 to crassulacean acid metabolism. *Journal of Plant Physiology* **262**: 153448.

Wang X, Kraatz B, Meng J, Carrapa B, Decelles P, Clementz M, Abdulov S, Chen FH. **2016**. Central Asian aridification during the late Eocene to early Miocene inferred from preliminary study of shallow marine-eolian sedimentary rocks from northeastern Tajik Basin. *Science China Earth Sciences* **59**: 1242–1257.

Wang H, Wu F, Yang L, Fang X. **2023**. Miocene lake evolution in the western Qaidam Basin, northern Tibetan Plateau: Evidence from aquatic-plant pollen. *Journal of Asian Earth Sciences* **250**: 105634.

Winter K, Holtum JAM. **2024**. Shifting photosynthesis between the fast and slow lane: Facultative CAM and water-deficit stress. *Journal of Plant Physiology* **294**: 154185.

Winter K, Smith JAC. **2022**. CAM photosynthesis: the acid test. *New Phytologist* **233**: 599–609.

Woodward FI. 1987. Stomatal numbers are sensitive to increases in CO2 from preindustrial levels. *Nature* **327**: 617-618.

Woodward FI, Bazzaz FA. 1988. The responses of stomatal density to CO2 partial pressure. *Journal of Experimental Botany* **39**: 1771-1781.

Woodward FI, Kelly CK. 1995. The influence of CO2 concentration on stomatal density. *New Phytologist* **131**: 311-27.

Supporting information

Supporting Information File. This file contains **Supporting Information Figs. S1-S7, Supporting Information Tables S1, S2** and **Supporting Information Notes S1-S4.**

Supporting Information Dataset S1. The model file in excel format.

Supporting Information Dataset S2. The model file in sbml format.

Supporting Information Dataset S3. Python scripts for all the simulations.

Supporting Information Dataset S4. Flux solutions i) for each step of C_3-to-CAM transition due to changes in atmospheric conditions between early-Eocene to early-Miocene and ii) for each point of the transition due to reduced transpirational water loss studied at each step of the atmospheric changes.

Supporting Information Dataset S5. Flux solutions obtained from simulating the model with different T (22-35°C) and RH (30-70%) at a fixed $[CO_2]_a$ of 800 ppm.

Supporting Information Dataset S6. Flux solutions obtained from simulating the model under different reduced $[CO_2]_a$ values at fixed T (35°C) and RH (70%).

Supporting Information Dataset S7. Correlation values of each reaction i) with change in atmospheric conditions (reduced $[CO_2]_a$, T and RH) between early-Eocene to early-Miocene and ii) with reduced transpirational water loss at each step of the atmospheric changes between that geological time interval.

Supporting Information Dataset S8. Flux solutions obtained from simulating the model by reducing RH from 80% to 40% with different combinations of T (26-35°C) and $[CO_2]_a$ (800, 419 and 250 ppm), either keeping the water loss free or keeping the water loss fixed at a value obtained with 80% RH for the corresponding T and $[CO_2]_a$ values.

Supporting Information Dataset S9. Flux solutions obtained from simulating the model i) at 80% RH without compromising the phloem sap production and ii) with RH reduced from 70% to 40% along with a reduced phloem sap at different T (26-35°C) under a fixed $[CO_2]_a$ of 250 ppm, either keeping the water loss free or keeping the water loss fixed at a value obtained with 80% RH for the corresponding T.

Supporting Information Dataset S10. The model file including additional osmolytes (nitrate, glucose, fructose and maltose) and transfer metabolites (glucose and malate) in excel format.

Supporting Information Dataset S11. Flux solutions by simulating the model with additional osmolytes and transfer metabolites i) for each step of C_3-to-CAM transition due to changes in atmospheric conditions between early-Eocene to early-Miocene and ii) for each point of the transition due to reduced transpirational water loss studied at each step of the atmospheric changes.

Supporting Information Dataset S12. Flux solutions by simulating the model under the changing atmospheric condition between early-Eocene to early-Miocene with the dual optimization function (maximization of phloem sap production followed by minimization of cellular economy) and the ratio of RuBisCO's carboxylase-to-oxygenase activity fixed at 3:1.

Supporting Information Dataset S13. Flux solution by simulating the model under the atmospheric condition of early-Eocene with the dual optimization function (maximization of phloem sap production

followed by minimization of cellular economy) and the ratio of RuBisCO's carboxylase-to-oxygenase activity fixed at 5.15:1.

Supporting Information Dataset S14. Flux solutions by simulating the model under the changing atmospheric condition between early-Eocene to early-Miocene with the dual optimization function (maximization of phloem sap production followed by minimization of cellular economy) and the changing ratio of RuBisCO's carboxylase-to-oxygenase activity from 3:1 to 5.15:1.

Supporting Information Fig. S1. Schematic representation of the model and constraints and flowcharts for simulating the model.

Supporting Information Fig. S2. Variation in the diffusion coefficient of CO_2 (D_{CO_2}) with temperature (T).

Supporting Information Fig. S3. Change in stomatal aperture size in different phases of day and night.

Supporting Information Fig. S4. Change in the CO_2 uptake at day and night.

Supporting Information Fig. S5. Variations in flux values of different carboxylating and decarboxylating enzymes.

Supporting Information Fig. S6. Variation in starch-malate cycle.

Supporting Information Fig. S7. The change in water-use efficiency (WUE) at different $[CO_2]_a$ and transpirational water loss.

Supporting Information Table S1. Different constraints used for GC and MC throughout the C_3-CAM transition.

Supporting Information Table S2. Comparison of flux values through some specific reactions of CAM under different $[CO_2]_a$ values.

Supporting Information Note S1. Increased flux of TCA cycle enzymes and O_2 uptake with the emergence of CAM.

Supporting Information Note S2. Capturing possible changes in temporal differential activities of metabolic enzymes and transporters during early-Eocene to early-Miocene time period.

Supporting Information Note S3. Simulating C_3 and CAM under predicted atmospheric changes in future.

Supporting Information Note S4. Simulating the model considering all potential osmolytes and transfer metabolites.

Acknowledgements

DS thanks Department of Biotechnology, Government of India for her fellowship.

Competing interests

The authors declare that there is no competing interest.

Author contributions

DS and SK designed the study, DS performed the simulations, both interpreted the results and co-wrote the paper.

Figures with legends

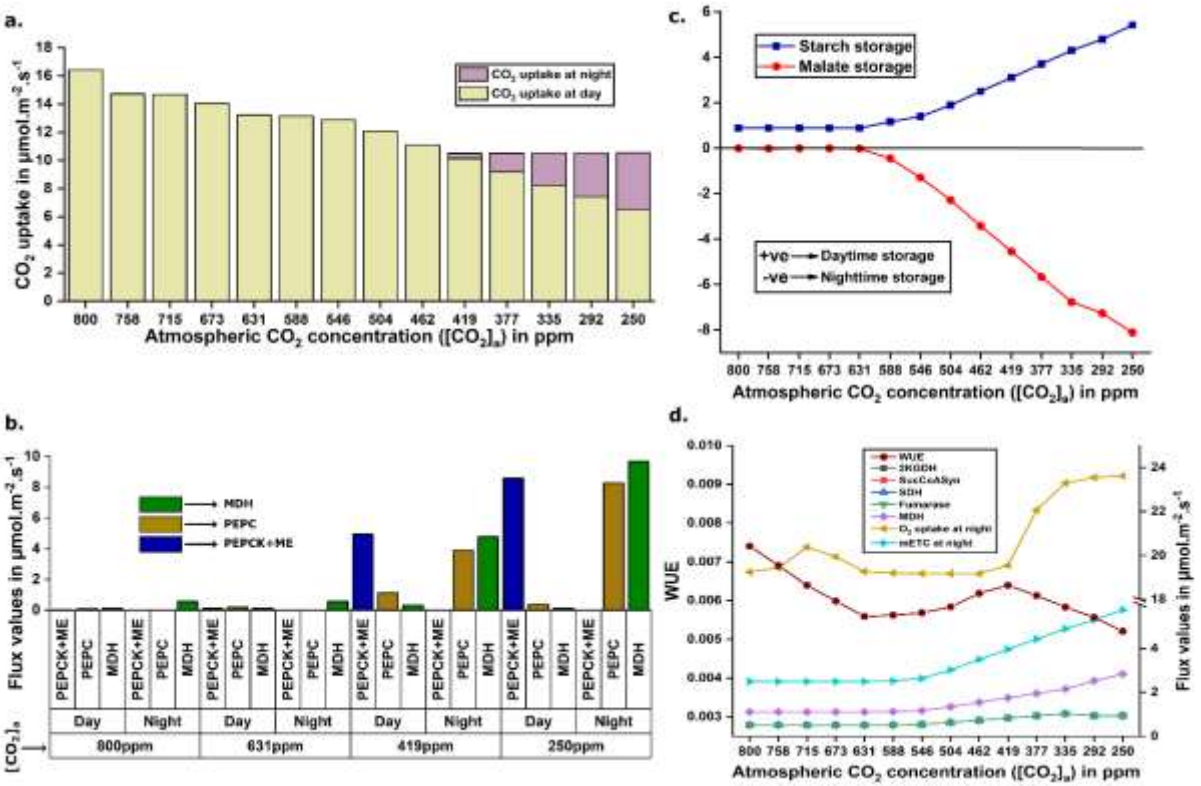

Fig. 1. Reduced $[CO_2]_a$ can induce CAM. **a.** Variation in the total CO_2 uptake throughout the diel cycle and the amount of CO_2 uptake at day and night with the decrease in $[CO_2]_a$. Total CO_2 uptake declined due to refixation of respiratory CO_2 (discussed in detail in main text). **b.** Changes in the activities of four C_4-like enzymes related to carboxylation (PEPC and MDH) and decarboxylation (PEPCK and ME) of malate at night and day respectively with the decline in $[CO_2]_a$ that show the metabolic shift towards CAM. **c.** The graph demonstrates that the daytime starch storage and the nighttime malate storage are increased throughout the C3-to-CAM transition (high to low $[CO_2]_a$). **d.** Flux through mETC and 5 enzymes of TCA cycle in MC and changes in WUE, total nocturnal O_2 uptake at night are shown. Flux values of 2KGDH, SucCoASyn, SDH and fumarase overlap. Only $[CO_2]_a$ values are shown in all the graphs. Corresponding T and RH values are listed in **Supporting Information Fig. S1c**.

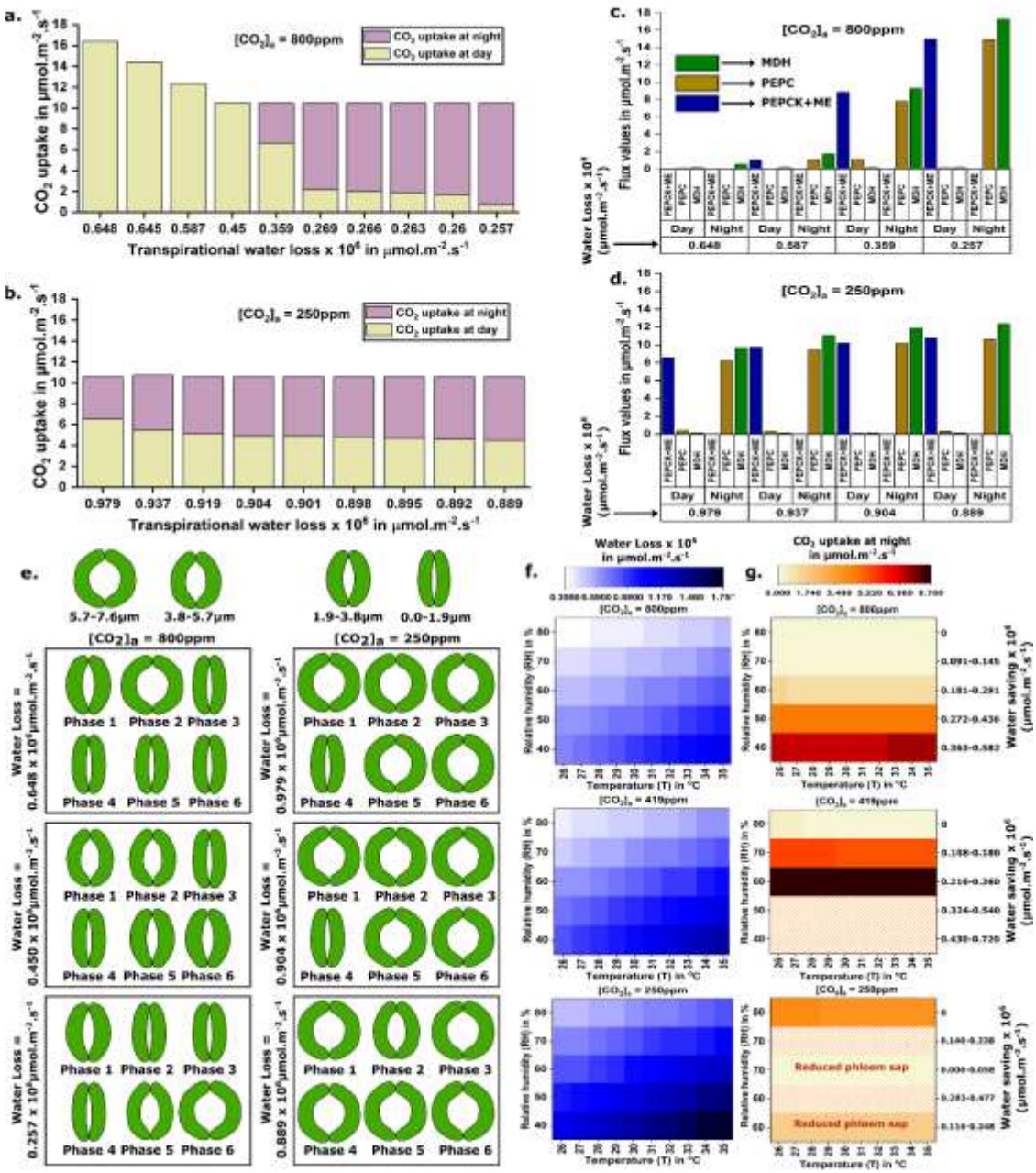

Fig. 2. a-b show the variation in CO_2 uptake at day and night with reduction in transpirational water loss at different $[CO_2]_a$. **c-d** show the changes in the activities of the carboxylating (PEPC and MDH) and decarboxylating (PEPCK and ME) enzymes with reduced transpirational water loss at different $[CO_2]_a$. **e.** Variations in stomatal aperture sizes at day and night with decline in $[CO_2]_a$ (row-wise) and transpirational water loss (column-wise) are shown. Reduced $[CO_2]_a$ forces the nighttime stomatal opening along with day, however, at a fixed $[CO_2]_a$, stomatal opening shifts from day to night with the decrease in transpirational water loss. **f.** Variation in transpirational water loss in different combinations of $[CO_2]_a$, T and RH. Water loss increases with decrease in $[CO_2]_a$, RH and increase in T. **g** shows that for a fixed T and $[CO_2]_a$, maintaining constant transpirational water loss leads to increase in nocturnal CO_2 uptake with decreasing RH, indicating the emergence of CAM under increasing aridity. Moreover,

at lower CO_2, increasing aridity (reducing RH) forces the plant to reduce its phloem sap production, showing a trade-off between water saving and phloem sap production. Only $[CO_2]_a$ values are shown in the graphs (a-e). Corresponding T and RH values are listed in **Supporting Information Fig. S1c**.